Generalized Transition State Theory. Canonical Variational Calculations Using the Bond Energy-Bond Order Method for Bimolecular Reactions of Combustion Products

Bruce C. Garrett and Donald G. Truhlar*

Contribution from the Department of Chemistry, University of Minnesota, Minneapolis, Minnesota 55455. *Received February 24, 1979*

Abstract: Canonical variational transition state theory is applied to a set of 37 atom-diatom reactions involving transfer of halogens, first-row atoms, and Al to survey the effect of varying the location of the generalized transition state on thermal rate constants. Potential energy surfaces are generated by a reduced-variable bond energy-bond order method. Rate constants are calculated by maximizing the generalized free energy of activation using a formalism presented in a previous paper. The average ratio of the conventionally calculated rate to the canonical variational one increases from 1.2 at 200 K to 2.1 at 4000 K. The error is generally larger for systems with relatively loose saddle points, although all the systems we consider here have bound bending modes at the saddle point. Ten representative systems are discussed in detail to illustrate the roles of various degrees of freedom in determining the effects.

Introduction

In previous articles, we have applied the canonical variational theory—a form of generalized transition state theory in which the dividing surface on which the transition-state assumption is applied is varied to minimize the calculated thermal rate constant—to collinear atom-diatom reactions[1,2] and to atom-diatom reactions in three dimensions.[3] In the first study of collinear reactions we used purely classical mechanics and considered six reactions. Classical canonical variational theory gives an upper bound on the exact classical mechanical equilibrium rate constant which is always as good as or better than the bound provided by classical conventional transition state theory. We showed by actual calculations that we could use a Morse-curve vibrational model to perform canonical variational theory calculations efficiently and that the improvement over conventional transition state theory was significant. For example, for the six reactions studied the average error at 1000 K in conventional transition state theory was 57% and the average error in canonical variational theory was 36%. At 300 K these average errors were 18 and 5%, respectively. In the second study of collinear reactions we used quasi-classical quantization of internal energies and quantal corrections[4] on reaction-coordinate motion and compared to accurate quantum mechanical rate constants; we considered three reactions and some isotopic analogues and considered five potential energy surfaces for a total of 12 systems. There is no longer a rigorous bound when quantum mechanical effects are included, and in 10 of the 12 cases both versions of transition-state theory without quantal corrections on reaction coordinate motion underestimated the thermal rate constant at 300 K. But hard-to-estimate quantal effects like tunneling and nonclassical reflection become less important at higher temperature, and, for the ten systems where accurate quantal results were available for 1000 K for comparison, conventional transition state theory and canonical variational theory, both without quantal corrections on reaction coordinate motion, had average errors of 38 and 13%, respectively. Including a simple estimate of the extent of tunneling by the lowest order Wigner correction factor changes these average errors to 45 and 9%, respectively. Thus using a variational criterion to locate the generalized-transition-state dividing surface can lead to significant improvement in a quantum-mechanical world too.

In the previous study of three-dimensional reactions we again used quantized partition functions, and we made a survey of 36 hydrogen-atom-transfer reactions. In all cases the potential energy surface was estimated by the bond energy-bond order (BEBO) method.[3,5,6] Again we found large effects of varying the dividing surface; for the 36 systems at 1000 K, the conventional transition state theory rate constant exceeded the canonical variational one by an average factor of 2.5 at 1000 K. In the present article we extend this survey to atom transfer reactions involving transfer of F, Cl, Br, I, C, N, O, Al, and B.

As pointed out by Mayer et al.,[7] the number of high-temperature reactions of interest is much greater than the number for which rate-constant measurements have been made. For this reason they used a reduced-variable BEBO method (RVBEBO) and conventional transition state theory to estimate the rate constants for many such reactions, involving both transfer of H and transfer of other atoms.[7-10] In this article we consider 37 reactions involving transfer of halogens, first-row atoms, and Al to see if variation of the dividing surface has a significant effect on the calculated rate constant. We also consider this set of 37 reactions as a sample with which to assess the general size and nature of the effects of varying the dividing surface on generalized transition state theory calculations for reactions involving transfer of nonhydrogen atoms. We wish to provide a general guide to these effects for a wide variety of conditions so we consider the temperature range 200-4000 K. The higher part of this temperature range is important for the burning of propellants.

Reactions Considered and Potential Energy Surfaces

The general reaction is denoted A + BC → AB + C. The RVBEBO method is applied using the AC repulsive interaction derived by Mayer et al.[7] in the formalism of ref 3. The data necessary for the calculations are bond energies D_e, bond lengths r_e, and vibrational frequencies ω_e for the diatomic fragments AB, AC, and BC, and the well depths and positions of the minima in the rare gas and mixed rare gas van der Waals complexes. D_e, r_e, and ω_e were taken to be those values used by Johnston and Parr[5] and Mayer et al.[7] In a few cases the required values were not given in ref 5 or 7 and the values[11-14] used in those cases are given elsewhere.[15] For the rare-gas data we used the values[16] assumed by Johnston and Parr[5] and Mayer et al.[7] for consistency with their work. We consider 31 of the 35 cases in Table I of ref 7; we do not consider the four reactions involving Be atoms since the RVBEBO method may be inappropriate for reactions of singlet atoms. In addition, we have added six reactions to their list to make the sample more

0002-7863/79/1501-5207$01.00/0

Table I. Detailed Quantities Characterizing the Various Endoergic and Thermoneutral Reactions for Generalized Transition State Theory Calculations at Three Choices of Dividing Surface: the Saddle Point, and the Canonical Variational Transition States for $T = 300$ and 4000 K

system A + BC[d]	quantal endoergicity,[e] kcal/mol	skew angle,[f] deg	generalized transition state properties[a]								comparison of conventional and canonical variational transition state theory[b]					Arrhenius parameters[c]	
											Q/Q^{CVT}						
			n_{AB}[g]	Δr_{AB},[h] a_0	Δr_{BC},[i] a_0	V_{MEP},[j] kcal/mol	$\hbar\omega_{st}$,[k] cm^{-1}	$\hbar\omega_b$,[l] cm^{-1}	$\Phi_{ip}(T)$,[m] deg	$\kappa^W(T)$[n]	bends[o]	rot.[p]	stretch[q]	$e^{\Delta V/k_BT}$ [r]	$k^{\ddagger}(T)/k^{CVT}(T)$	E_a, kcal/mol	A, cm^3/molecule·s
O + Fl	1.1	51	0.149	0.93	0.08	1.0	574	60	150, 93	1.01						2.95	5.95×10^{-11}
			0.170	0.87	0.09	1.0	562	62	151		1.06	1.01	0.97	0.99	1.02	2.92	5.58×10^{-11}
			0.695	0.18	0.58	−1.0	793	73	98		1.34	0.99	1.39	0.78	1.45		
H + AlCl	4.3	82	0.459	0.38	0.31	6.4	1127	171	157, 103	1.10						11.38	7.76×10^{-11}
			0.521	0.32	0.36	6.3	1217	173	157		1.03	0.98	1.24	0.90	1.13	11.42	7.36×10^{-11}
			0.608	0.25	0.46	6.0	1327	175	106		1.05	0.94	1.18	0.96	1.12		
Cl + BCl	0	40	0.500	0.34	0.34	6.3	301	90	155, 103	1.08						5.59	1.00×10^{-10}
			0.360	0.50	0.22	4.3	591	88	154		0.96	0.99	2.47	0.73	1.71	5.55	5.53×10^{-11}
			0.285	0.62	0.16	4.1	705	86	101		0.93	0.96	2.35	0.94	1.98		
Cl + CCl	0	42	0.500	0.34	0.34	3.6	305	80	153, 100	1.06						4.64	1.12×10^{-10}
			0.348	0.52	0.21	3.4	599	78	153		0.95	0.99	2.48	0.74	1.74	4.62	6.29×10^{-11}
			0.278	0.63	0.16	3.2	698	75	97		0.92	0.96	2.29	0.95	1.93		
C + ClC	0	75	0.500	0.34	0.34	6.2	520	75	156, 104	1.07						7.37	8.66×10^{-11}
			0.500	0.34	0.34	6.2	520	75	156		1.00	1.00	1.00	1.00	1.00	7.37	8.66×10^{-11}
			0.684	0.19	0.57	5.7	630	73	102		0.95	0.98	1.21	0.95	1.07		
H + CF	4.0	77	0.527	0.32	0.37	14.6	2051	271	158, 108	1.42						18.78	6.10×10^{-11}
			0.565	0.28	0.41	14.5	2150	272	158		1.02	0.98	1.26	0.90	1.13	18.85	6.08×10^{-11}
			0.591	0.26	0.44	14.4	2211	273	108		1.02	0.96	1.08	0.98	1.04		
Cl + BF	2.3	46	0.654	0.21	0.52	4.1	578	94	152, 97	1.09						7.76	1.13×10^{-10}
			0.706	0.17	0.60	4.0	684	92	152		0.95	0.99	1.32	0.93	1.15	7.80	1.04×10^{-10}
			0.326	0.55	0.19	2.6	1071	96	95		1.03	0.98	1.86	0.82	1.55		
H + BCl	18.6	75	0.737	0.15	0.66	5.2	2048	241	156, 105	1.09						24.76	6.57×10^{-11}
			0.753	0.11	0.69	5.2	2071	239	156		0.99	0.99	1.05	0.99	1.02	24.77	6.61×10^{-11}
			0.708	0.17	0.61	5.2	2005	243	106		1.01	1.02	0.98	1.00	1.01		
H + BF	20.9	77	0.742	0.15	0.67	5.7	2063	250	157, 106	1.13						27.74	9.88×10^{-11}
			0.752	0.14	0.68	5.7	2076	249	156		0.99	0.99	1.03	0.99	1.01	27.74	9.87×10^{-11}
			0.703	0.17	0.60	5.7	2004	253	107		1.02	1.04	0.97	0.99	1.02		
C + FH	29.3	82	0.811	0.10	0.82	8.0	1240	272	159, 113	1.75						39.21	6.68×10^{-11}
			0.741	0.15	0.66	7.7	1573	296	160		1.22	0.99	2.21	0.57	1.52	39.28	4.97×10^{-11}
			0.600	0.25	0.45	5.4	2348	330	116		1.42	0.94	1.93	0.72	1.87		
Cl + ClI	22.6	76	0.852	0.08	0.94	4.8	761	198	156, 104	1.55						29.09	1.61×10^{-10}
			0.805	0.11	0.80	4.6	857	214	157		1.18	1.00	1.27	0.77	1.15	28.94	1.09×10^{-10}
			0.602	0.25	0.45	1.5	1670	256	109		1.56	0.95	2.22	0.66	2.20		
Br + OF	0.6	48	0.899	0.05	1.13	0.6	651	46	140, 74	1.01						2.67	1.59×10^{-10}
			0.849	0.08	0.93	0.6	633	52	143		1.22	1.04	0.95	0.93	1.13	2.59	1.24×10^{-10}
			0.304	0.58	0.18	−1.4	788	63	85		1.50	1.06	1.22	0.77	1.50		
Br + NH	16.0	76	0.901	0.05	1.14	3.1	649	176	154, 101	1.30						20.97	2.10×10^{-10}
			0.834	0.09	0.88	2.8	800	205	156		1.37	1.00	1.47	0.59	1.19	20.63	9.91×10^{-11}
			0.594	0.26	0.44	−0.9	1968	259	109		1.95	0.94	3.11	0.60	3.42		
Cl + FB	40.1	61	0.914	0.04	1.20	6.1	772	108	160, 116	1.06						48.12	6.31×10^{-11}
			0.907	0.05	1.16	6.1	768	110	160		1.03	1.01	0.99	0.98	1.01	48.08	5.87×10^{-11}
			0.855	0.08	0.95	5.6	736	120	119		1.20	1.05	0.96	0.94	1.05		

H + BrAl	12.4	87	0.940	0.03	1.38	4.7	2580	187	155, 98	1.01						17.94	5.52×10^{-11}
			0.933	0.03	1.33	4.7	2571	189	155		1.03	1.02	0.93	0.99	1.01	17.88	4.98×10^{-11}
			0.832	0.09	0.88	4.0	2429	206	105		1.14	1.21	0.94	0.92	1.20		
Br + BrB	85.0	76	0.946	0.03	1.43	10.2	319	57	162, 119	1.06						97.00	7.81×10^{-11}
			0.943	0.03	1.41	10.2	319	58	162		1.02	1.00	1.00	0.99	1.01	96.98	7.54×10^{-11}
			0.922	0.04	1.25	9.9	313	61	121		1.09	1.02	0.98	0.96	1.05		
H + IAl	18.1	88	0.957	0.02	1.55	3.8	2267	145	145, 90	1.01						22.78	7.23×10^{-11}
			0.951	0.02	1.48	3.8	2260	148	148		1.03	1.02	0.98	0.98	1.02	22.74	6.56×10^{-11}
			0.882	0.06	1.05	3.1	2179	162	97		1.16	1.17	0.96	0.91	1.19		
Cl + ClB	39.7	70	0.961	0.02	1.59	3.0	556	53	154, 99	1.02						44.27	1.29×10^{-10}
			0.953	0.02	1.50	2.9	554	55	154		1.08	1.02	0.99	0.96	1.05	44.22	1.12×10^{-10}
			0.903	0.05	1.14	2.1	535	64	107		1.28	1.08	0.96	0.90	1.20		
Cl + ClAl	14.3	62	0.962	0.02	1.60	2.6	556	43	153, 97	1.01						18.29	7.22×10^{-11}
			0.950	0.03	1.48	2.6	553	45	154		1.09	1.03	0.99	0.95	1.06	18.22	6.07×10^{-11}
			0.881	0.07	1.05	1.8	530	52	105		1.25	1.12	0.95	0.91	1.22		
Br + FC	55.3	56	0.962	0.02	1.61	2.1	667	61	156, 94	1.02						59.00	1.41×10^{-10}
			0.955	0.02	1.53	2.1	666	63	156		1.11	1.02	1.00	0.95	1.07	58.93	1.17×10^{-10}
			0.895	0.05	1.11	0.9	647	78	104		1.42	1.10	0.97	0.87	1.32		
Cl + ClC	21.6	69	0.964	0.02	1.63	1.5	557	41	148, 87	1.01						24.67	1.78×10^{-10}
			0.950	0.03	1.47	1.5	553	44	149		1.14	1.03	0.99	0.93	1.09	24.58	1.41×10^{-10}
			0.884	0.06	1.06	0.6	527	53	98		1.36	1.10	0.95	0.90	1.28		
Al + ClH	30.7	84	0.964	0.02	1.64	4.2	472	132	155, 100	1.21						36.85	3.84×10^{-10}
			0.957	0.02	1.54	4.2	470	138	155		1.09	1.00	1.00	0.96	1.04	36.78	3.29×10^{-10}
			0.708	0.17	0.60	−2.5	1393	208	109		2.22	0.97	3.00	0.43	2.78		
F + FC	68.6	64	0.968	0.02	1.69	1.6	866	65	147, 87	1.02						71.65	1.35×10^{-10}
			0.958	0.02	1.56	1.6	863	70	149		1.14	1.04	0.99	0.93	1.09	71.55	1.06×10^{-10}
			0.894	0.06	1.10	0.07	833	88	101		1.53	1.17	0.97	0.83	1.43		
Cl + OH	60.6	78	0.975	0.013	1.81	1.8	858	130	150, 92	1.16						64.16	3.26×10^{-10}
			0.966	0.02	1.66	1.7	852	142	151		1.19	1.01	0.98	0.93	1.10	64.06	2.51×10^{-10}
			0.774	0.13	0.73	−6.1	1270	253	111		3.04	1.02	1.52	0.37	1.74		
Cl + FH	75.8	80	0.978	0.011	1.88	1.9	786	129	150, 92	1.17						79.40	3.26×10^{-10}
			0.971	0.015	1.74	1.8	781	142	152		1.19	1.01	0.99	0.92	1.10	79.29	2.51×10^{-10}
			0.807	0.11	0.81	−6.3	1195	255	112		3.10	1.02	1.55	0.36	1.76		
O + ClC	30.0	74	0.981	0.010	1.94	0.7	861	36	137, 66	1.01						32.04	2.10×10^{-10}
			0.965	0.02	1.65	0.6	855	41	142		1.29	1.07	0.98	0.88	1.19	31.89	1.38×10^{-10}
			0.886	0.06	1.07	−0.8	812	55	89		1.61	1.23	0.95	0.84	1.57		
Br + FH	84.6	78	0.984	0.008	2.04	1.6	668	114	148, 88	1.13						87.99	4.65×10^{-10}
			0.978	0.011	1.87	1.5	664	126	150		1.22	1.01	0.99	0.91	1.11	87.89	3.47×10^{-10}
			0.820	0.10	0.84	−7.8	1127	240	110		3.43	1.02	1.73	0.31	1.86		
Cl + ClH	45.0	83	0.992	0.004	2.37	0.7	563	69	140, 72	1.05						47.53	7.63×10^{-10}
			0.985	0.008	2.05	0.7	561	83	145		1.42	1.01	0.99	0.86	1.22	47.37	4.71×10^{-10}
			0.780	0.12	0.74	−8.7	1103	180	105		4.46	1.01	2.00	0.30	2.74		
F + FH	97.9	81	0.993	0.003	2.47	0.4	874	70	132, 59	1.05						99.94	7.76×10^{-10}
			0.986	0.007	2.08	0.3	871	91	140		1.62	1.04	0.99	0.81	1.35	99.73	4.03×10^{-10}
			0.931	0.04	1.32	−2.5	835	158	94		3.39	1.10	0.97	0.69	2.49		
Br + BrH	41.2	85	0.993	0.003	2.47	0.7	327	57	138, 68	1.04						43.87	1.11×10^{-9}
			0.987	0.007	2.12	0.6	326	69	69		1.44	1.00	0.99	0.85	1.23	43.70	6.78×10^{-10}
			0.797	0.11	0.78	−8.0	1036	147	101		4.26	0.98	3.26	0.34	4.60		
Cl + IH	21.0	88	0.995	0.003	2.57	0.5	384	51	137, 65	1.03						23.41	1.13×10^{-9}
			0.986	0.007	2.11	0.4	382	66	143		1.61	1.01	0.99	0.82	1.32	23.20	6.01×10^{-10}
			0.709	0.17	0.61	−7.9	1158	149	104		5.00	0.97	3.10	0.35	5.18		

Table I. (*Continued*)

system A + BC[d]	quantal endoergicity,[e] kcal/mol	skew angle,[f] deg	generalized transition state properties[a]								comparison of conventional and canonical variational transition state theory[b]					Arrhenius parameters[c]	
											Q/Q^{CVT}						
			n_{AB}[g]	Δr_{AB},[h] a_0	Δr_{BC},[i] a_0	V_{MEP},[j] kcal/mol	$\hbar\omega_{st}$,[k] cm^{-1}	$\hbar\omega_b$,[l] cm^{-1}	$\Phi_{tp}(T)$,[m] deg	$\kappa^W(T)$[n]	bends[o]	rot.[p]	stretch[q]	$e^{\Delta V/k_BT}$ [r]	$k^{\ddagger}(T)/k^{CVT}(T)$	E_a, kcal/mol	A, cm^3/molecule·s
F + FB	62.4	65	0.995	0.003	2.58	0.2	874	28	118, 34	1.00						64.01	6.50×10^{-10}
			0.982	0.009	1.99	0.2	871	41	132		1.84	1.17	0.99	0.75	1.61	63.76	2.63×10^{-10}
			0.913	0.05	1.20	−2.5	845	68	85		2.66	1.45	0.98	0.72	2.72		
F + BrH	36.7	87	0.996	0.002	2.67	0.2	669	44	127, 48	1.02						38.63	8.80×10^{-10}
			0.985	0.007	2.07	0.2	665	66	139		2.01	1.03	0.99	0.76	1.55	38.37	3.69×10^{-10}
			0.746	0.14	0.67	−8.5	1141	161	103		6.53	1.02	1.75	0.33	3.88		
F + ClH	43.3	84	0.996	0.002	2.69	0.3	792	48	127, 48	1.02						45.16	8.49×10^{-10}
			0.986	0.007	2.10	0.08	788	72	138		1.99	1.04	0.99	0.76	1.56	44.90	3.53×10^{-10}
			0.765	0.13	0.71	−9.0	1151	179	103		6.84	1.07	1.48	0.31	3.38		
F + ClB	38.0	73	0.997	0.002	2.79	0.10	792	17	107, 15	1.00						39.36	6.29×10^{-10}
			0.983	0.008	2.00	−0.10	787	27	127		2.13	1.20	0.99	0.73	1.83	39.11	2.24×10^{-10}
			0.913	0.04	1.20	−2.1	756	45	77		2.28	1.45	0.96	0.76	2.39		
I + IH	34.9	86	0.998	0.001	3.00	0.3	216	37	128, 51	1.02						37.34	2.60×10^{-9}
			0.993	0.003	2.44	0.3	216	50	136		1.69	1.00	1.00	0.81	1.36	37.13	1.33×10^{-9}
			0.805	0.11	0.80	−9.3	922	121	95		5.15	0.98	4.40	0.30	6.69		
Br + BrCl	5.7	67	*s*	*s*	*s*	*s*	*s*	*s*	*s*	*s*						6.03[t]	9.58×10^{-10} [t]
			0.998	0.001	2.98	−0.4	328	52	89		*s*	*s*	*s*	*s*	1.95[t]	6.16	6.13×10^{-10}
			0.967	0.02	1.68	−2.5	325	121	47		*s*	*s*	*s*	*s*	2.40[t]		

[a] For each reaction the three lines are for three locations of the generalized transition state: the saddle point location $s = 0$ and the canonical variational transition state location $s_*^{CVT}(T)$ for $T = 300$ and 4000 K, respectively. [b] For each reaction the two lines are for temperatures of 300 and 4000 K, respectively. [c] For the temperature range 300–1000 K. For each reaction the two lines are for conventional and canonical variational transition state theory, respectively. [d] In all cases reaction occurs with the atom written first in the diatomic. For homonuclear diatomics the rate calculated is the sum of the reaction with both ends. [e] From zero-point level to zero-point level. [f] The angle between the r_{AB} and r_{BC} axes in the (x, y) coordinate system which diagonalizes the kinetic energy. [g] AB bond order at each generalized transition state. [h] Change in the AB bond length as compared to products ($r_{AB} - r_e^{AB}$) for a value for r_{AB} on minimum energy path at each generalized transition state location of s. [i] Change in the BC bond length as compared to reactants ($r_{BC} - r_e^{BC}$) for a value of r_{BC} on the minimum energy path at each generalized transition state location of s. [j] Potential energy at each generalized transition state relative to zero at the bottom of the asymptotic product vibrational well; for saddle-point location of generalized transition state this is intrinsic barrier height. [k] Planck's constant times the vibrational frequency for the stretching degree of freedom at each generalized transition state. [l] Planck's constant times the vibrational frequency for the bending degree of freedom at each generalized transition state. [m] Computed bond angle at the classical turning point of bending motion with k_BT of energy per degree of freedom. The two entries $\Phi_{\ddagger tp}(T)$ for the saddle point location of the generalized transition state are for 300 and 4000 K, respectively. [n] Wigner tunneling correction factor at 300 K. [o] Square of the ratio of bending partition functions. [p] Ratio of rotational partition functions. [q] Ratio of stretching partition functions. [r] $\exp\{-[V_{MEP}(s = 0) - V_{MEP}(s = s_*^{CVT})]/k_BT\}$. [s] For this reaction there is no saddle point and therefore these values are not computed. [t] For these quantities the Gorin model[3] is used in place of conventional transition state theory. For the Gorin model calculations, the long-range interaction between Cl and Br_2 is assumed to be $V \sim -287x^{-6}$ in hartree atomic units where x is the Cl to Br_2 distance.

representative of the full range of reaction types. The reactions considered by Mayer et al.[7] are a survey of systems of interest in connection with the behavior of flames, shock waves, plasmas, and rocket-propellant gases, but the authors excluded many diatomic species whose molecular parameters were relatively uncertain or whose bonding was predominantly ionic, and they also excluded several reactions because the computed bending partition functions were too low for the bending degree of freedom to be treated using small-vibration theory in conventional transition-state theory. Even for systems where the bonding is predominantly covalent, the RVBEBO method predictions may be quantitatively unreliable, and alternative assumptions in the theory may lead to large differences in the predicted barrier height.[17] Our purpose here is to test the differences between conventional and canonical variational transition state theories for a range of given potential energy surfaces and atomic masses, so the quantitative accuracy of the potential surfaces is not of primary concern. For the results to be interesting, we require only that the surfaces be reasonably realistic, i.e., representative of surface types that might actually occur.[3] The potential surfaces for reactions involving C may be better approximations for reactions of CH_3 than for C itself. Similarly some of the other potential surfaces might also be considered better as general types than as accurate approximations for the atoms nominally considered.

The reactions considered in this paper are listed (in the endoergic direction for nonthermoneutral reactions) in Table I in order of increasing saddle-point bond order $n^{\ddagger}_{AB}$ of the new bond. In all cases the masses used are those for the most abundant naturally occurring isotope. For each reaction, the first line gives the zero-point-to-zero-point endoergicity, the skew angle of the scaled and skewed coordinate system[6] which diagonalizes the collinear kinetic energy, and several properties of the conventional transition state. The differences $\Delta r^{\ddagger}_{AB}$ and $\Delta r^{\ddagger}_{BC}$ in AB and BC bond lengths between the saddle point and the product value of the AB bond length and reactant value of the BC bond length are given to indicate the symmetry (or lack thereof) of the location of the saddle point. The value V_{MEP} ($s = 0$) of the classical potential energy at the saddle point measured relative to zero of energy at the bottom of the product vibrational well and the saddle point values of the vibrational frequencies, the transverse stretching motion, and the bending motion are also given. The value $\Phi_{\ddagger tp}(T)$ of the classical turning point for the bending motion in the mixed harmonic–quartic approximation to the bending potential with k_BT of energy per degree of freedom is given for temperatures of 300 and 4000 K. Since the saddle point is always linear (bond angle $\Phi = 180°$) in the RVBEBO approximation, this indicates the amplitude of oscillation for the bending motion with the average bending energies for these temperatures and is used as a test of the validity of the small vibrations approximation for the bending degrees of freedom. At 300 K $\Phi_{\ddagger tp}(T)$ is greater than 107° for all reactions and the mixed harmonic–quartic approximation to the RVBEBO bending potential should be quite good, as has been found[3,15] in other applications of the BEBO and RVBEBO methods. At 4000 K we find for all the systems that even at k_BT of energy per degree of freedom, the bending degree of freedom is bound ($\Phi_{\ddagger tp} > 0°$); however, for small values of $\Phi_{\ddagger}(T)$, e.g., the few values less than 90°, the validity of the small vibrations approximations is suspect. The lowest order Wigner tunneling correction[4,18] is given for 300 K to roughly indicate the importance or unimportance of tunneling in these systems. In all but four systems this factor is less than 1.2; its maximum value is 1.75. The second and third lines for each reaction and the last two numbers in the first line are explained in the Results section.

Theory

The generalized transition state theory calculations were carried out using the same formalism as in ref 3. In particular, the reaction coordinate s is measured in the x, y coordinate system [which is obtained from r_{AB}, r_{BC} one by skewing the latter axes to an angle

$$\beta = \arctan\left(\frac{m_B m_{ABC}}{m_A m_C}\right)^{1/2} \quad (1)$$

to diagonalize the collinear kinetic energy and scaling them to a reduced mass $m_A m_{BC}/(m_A + m_{BC})$] along the minimum energy path (path of steepest descent from the saddle point to reactants and products) with s positive on the product side of the saddle point and negative on the reactant side. Notice that by this convention the skew angle β tends to 90° as m_B becomes infinitely heavy, i.e., no skewing is required in that limit. Generalized transition states are dividing surfaces perpendicular to the reaction coordinate labelled by the value of s at which they intersect it. The CVT generalized transition state is the one that minimizes the thermal rate constant and maximizes the generalized free energy of activation. The conventional transition state is the one through the saddle point, which is located at $s = 0$. The value of s for the canonical variational transition state at temperature T is called $s_*^{CVT}(T)$. Rotation–vibration interaction and intermode vibrational coupling are neglected, stretching vibrations are treated as Morse curves, and quartic anharmonicity is included in the bending potential. We consider only one potential energy surface for each reaction, and we do not multiply our results by a multiple surface coefficient.[19]

Results

Table I gives a detailed comparison of conventional and canonical variational transition state theory for the 37 reactions considered here for two temperatures, 300 and 4000 K. For each reaction the first line is for conventional transition state theory and the second and third lines are for canonical variational transition state theory at these two temperatures, respectively. For the first line the first 11 columns were described in the previous section. The fourth through tenth entries describe the saddle point properties for each reaction. The first seven entries (columns four to ten) of the second and third lines give the same properties for the canonical variational transition state at 300 (line 2) and 4000 K (line 3). The locations of the CVT dividing surfaces are indicated by the value of the bond order n_{AB} of the new bond at the dividing surface as well as by the difference in AB and BC bond lengths between the value at the CVT dividing surface and the product value at the AB bond length and the reactant value of the BC bond length, respectively. These values should be compared with those given for the saddle point to see how far the CVT transition states are shifted from the conventional one. The next columns give properties of the potential energy surface at the CVT dividing surfaces: the value $V_{MEP}[s = s_*^{CVT}(T)]$ of the classical potential energy on the minimum energy path with zero of energy at products, the vibrational frequency of the transverse stretching motion, and the vibrational frequency of the bending motion. Also given is the value $\Phi_{CVTtp}(T)$ of the classical turning point for the bending motion in a mixed harmonic–quartic approximation to the RVBEBO bending potential with k_BT of energy per degree of freedom. The value Φ_{CVTtp} in the second line should be compared with the first value of $\Phi_{\ddagger tp}$ in the first line, and the value Φ_{CVTtp} in the third line should be compared to the second value of $\Phi_{\ddagger tp}$ in the first line. It should be noticed that, for cases where $\Phi_{\ddagger tp}$ is very small, e.g., for the F + ClB reaction at 4000 K, Φ_{CVTtp} at the same temperature is much larger.

The final seven columns of Table I compare the thermal rate constants calculated by conventional and canonical variational transition state theory. For each reaction, entries 8–11 in lines 2 (300 K) and 3 (4000 K) give a detailed comparison of the factors which contribute to the ratio $k^{\ddagger}(T)/k^{CVT}(T)$ of con-

ventional and canonical variation theory rate constants. These four factors are the ratios for two locations of the dividing surface—the saddle point and the canonical variational location—of generalized transition state partition functions for bending, rotation, and transverse stretching and of classical Boltzmann factors at the bottom of the transverse potential well. The product of these four factors is always greater than or equal to one and is equal to $k^{\ddagger}(T)/k^{CVT}(T)$. The energetic factor (the ratio of classical Boltzmann factors) always favors location of the dividing surface at the saddle point. It is unity if and only if the variational transition state occurs at the saddle point; it is less than unity for any other choice of dividing surface. The other three factors account for entropic effects; in general they favor a location of the dividing surface different from the saddle-point location. Always at least one of these factors is greater than or equal to unity, and often two or all three are greater than unity.

The last two columns of Table I give the Arrhenius parameters, the activation energy E_a and the preexponential factor A, determined from the calculated rate constants at 300 and 1000 K. The top and second lines for each reaction are for conventional and canonical variational transition state theory, respectively.

Discussion

Before giving a detailed discussion of a subset of the reactions we present some general trends as gleaned from Table I. First, for most reactions (the exception being a few of the reactions with relatively looser saddle points) the rotational partition function generally has only a small effect on the ratio of the conventional transition state theory rate constant to the canonical variational one. Second, the ratio of partition functions for the stretch and bend is correlated to the changes in vibrational frequency for these two degrees of freedom. If the vibrational frequency increases as the dividing surface is moved away from the saddle point, the energy levels also increase, which decreases the generalized partition function. Third, as the saddle point becomes more asymmetric the importance of the bending degree of freedom relative to the stretching degree of freedom in determining the location of the canonical variational dividing surface increases. The first 13 reactions in Table I have the 13 most symmetric saddle point positions; for these reactions the ratio of conventional transition state to CVT bend partition function is greater than that for the stretch in only two cases at 300 K. For the next 23 reactions, the bend ratio is greater than the stretch at 300 K. Within the subset of reactions with symmetric and near-symmetric saddle points the largest difference between conventional transition state theory and canonical variational theory rate constants is seen for the symmetric reactions. Also in these cases the CVT transition states tend to be shifted away from the saddle point toward less symmetric geometries closer to the endoergic products. As the saddle point is located further into the product asymptotic valley and the ratio of partition functions for the bends becomes larger than that for the stretch, the largest ratios of rate constants are seen in the systems with their saddle points furthest into the asymptotic valley. For these cases the CVT transition states are shifted away from products back toward more symmetric geometries.

Table II gives, for 36 of the reactions studied, the median ratio of the conventional transition state theory rate constant to the canonical variational one as a function of temperature. The median ratio is less than 25% for $T \leq 1000$ K but increases to 1.66 at 4000 K. Effects of individual systems are of course sometimes much larger.

We now consider some representative reactions in greater detail. For these cases plots of the generalized free energy of activation[3] as a function of the location of the dividing surface for four temperatures—1, 200, 600, and 2400 K—are shown in Figures 1-10. Also shown is the potential energy along the minimum-energy path. For sufficiently low temperatures, contributions to the generalized free energy of activation from the generalized vibrational partition functions come only from the zero-point energies and contributions from the rotational partition function are zero. At these low temperatures the generalized free energy of activation curves are equal to the ground-state vibrationally adiabatic (VAG) potential curve to within an additive constant. Thus the 1 K generalized free energy of activation curve is essentially identical with the VAG curve with its zero of energy at reactants. In each plot the location $s = 0$ corresponds to the conventional transition state, i.e., the saddle point. The CVT transition states are located at the maxima in the generalized free energy of activation curves. The sharp dips seen in the free-energy curves in four of the figures are due to sharp dips in the vibration energy levels of the stretch in the corner-turning region of the minimum-energy path through the r_{AB}, r_{BC} plane or the x, y plane where the x, y axes are obtained from r_{AB}, r_{BC} by scaling and skewing to achieve a diagonal kinetic energy with the same reduced mass in each direction. The dips only occur here in systems with relatively small skew angles; for the four cases where the plots show dips the skew angles are 51° or less. This phenomenon can be understood by considering the reduced mass for the stretching degree of freedom in r_{AB}, r_{BC} coordinates. The smallest skew angles occur in heavy-atom collisions with a light atom–heavy atom molecule ($\mathcal{H} + \mathcal{LH}$). Asymptotically the $\mathcal{LH}$ pair has a small reduced mass and high vibrational frequency. Consider the collision of a symmetric system (A + BA) in the r_{AB}, r_{BC} coordinate system. As the collision proceeds there will be a configuration where the light atom does not move in the transverse stretching motion, which becomes a symmetric stretch motion of the two heavy atoms. For this configuration the reduced mass is essentially equal to that for the two heavy atoms and is much larger than the asymptotic reduced mass. Therefore the vibrational frequency is much smaller for this symmetric stretch oscillation than for reactants or products. For systems which are not exactly symmetric the light atom always moves at least slightly in the transverse stretch and makes some contribution to the reduced mass. However, the qualitative effect is the same.

We consider the ten reactions selected for more detailed discussion in order of increasing saddle point new-bond bond orders $n^{\ddagger}_{AB}$. All reactions are considered in the endoergic or thermoneutral direction. Consider first the reaction O + FI. This reaction is unusual because it has an early barrier but is an endoergic reaction, i.e., it violates the Hammond[20] postulate. In the potential energy plot at the bottom of Figure 1, the potential goes to zero for $s = -\infty$ and to 0.6 kcal/mol for $s = +\infty$. Similarly the ground-state adiabatic potential curve (generalized free energy of activation curve for $T = 1$ K) goes to zero for $s = -\infty$ and to 1.1 kcal/mol for $s = +\infty$. For temperatures of 200-4000 K the CVT location of the dividing

Table II. Median and Average of the Ratios of Conventional and Canonical Variational Transition State Theory Rate Constants for 36 Reactions[a] at 8 Temperatures

T, K	median $k^{\ddagger}/k^{CVT}$	av $k^{\ddagger}/k^{CVT}$
200	1.11	1.21
300	1.12	1.22
400	1.12	1.24
600	1.17	1.30
1000	1.23	1.39
1500	1.29	1.49
2400	1.41	1.73
4000	1.66	2.11

[a] Cl + Br_2 excluded because it has no saddle point.

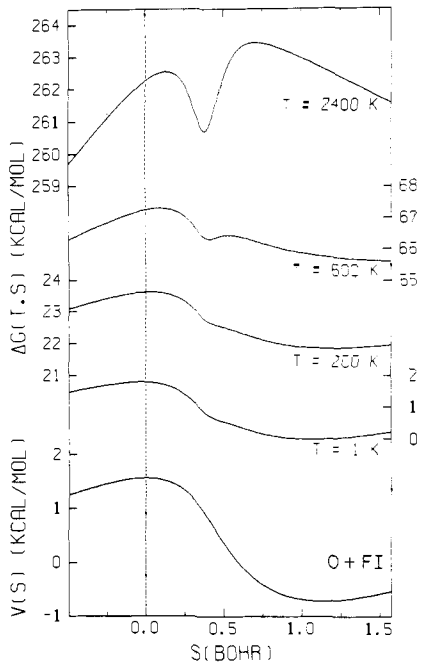

Figure 1. Classical potential energy barrier and generalized free energy of activation curves for the reaction O + FI → OF + I. The abscissa is the reaction coordinate in bohrs, and the dashed vertical line indicates the saddle-point location $s = 0$. The lowest curve is the classical potential energy along the minimum-energy reaction path with the zero of energy taken at the bottom of the reactant potential curve. The other four curves are generalized free energies of activation at temperatures of 1, 200, 600, and 2400 K for a standard state of 1 cm^3/molecule. For each of Figures 1–10, the reaction A + BC is thermoneutral or endothermic, and the range of reaction coordinate shown is from that corresponding to $n_{AB} = 0.05$ to that corresponding to $n_{AB} = 1 - 0.1n^{\ddagger}_{BC}$ where n_{AB} is AB bond order and $n^{\ddagger}_{BC}$ is BC saddle point bond order.

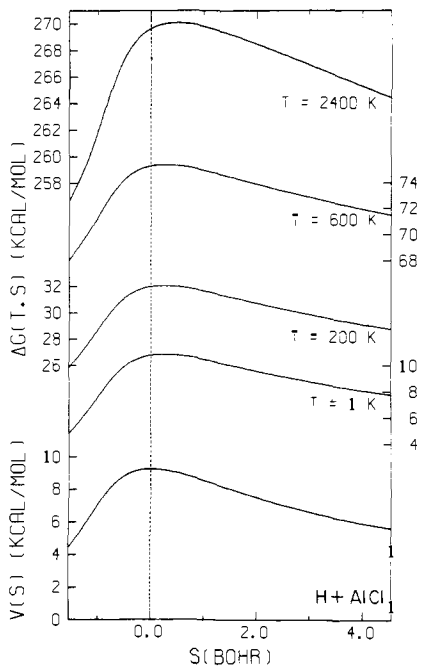

Figure 2. Same as Figure 1 except for H + AlCl → HAl + Cl.

surface is on the product side of the saddle point, i.e., s greater than zero. For temperatures in the range 200–1500 K the absolute maximum in the generalized free energy of activation curves is within $0.14a_0$ of the saddle point, and there is little difference between the values of the generalized free energy of activation at this location and at the saddle point. In Figure 1 a second local maximum in the free-energy curve appears for 600 K at $s = 0.53a_0$; however, it is not as high as the absolute maximum at $0.08a_0$. For 2400 K and above this second maximum becomes larger than the one nearer to the saddle point. For this reaction the stretching vibrational frequency decreases as the dividing surface is moved from the saddle point into the corner-turning region of the minimum-energy path, but the bending vibrational frequency increases because the generalized transition state becomes tighter. At low temperatures the bending and stretching degrees of freedom are competing, the bends favoring a dividing surface moved toward products and the stretch favoring one moved toward reactants. The bending degree of freedom dominates, and the CVT dividing surface is located on the product side of the saddle point. At higher temperatures, 2400 and 4000 K, the energetic factor becomes less important and the dividing surface can be located where the potential energy is much lower. At these temperatures the CVT dividing surface is located past the corner region where both the bending and the stretching vibrational frequencies are greater than at the saddle point. Thus for these temperatures the bending and stretching entropic factors reinforce one another and the ratio of rate constants is much larger than at lower temperatures. Because the conventional transition state theory and canonical variational theory predict such similar results for this reaction in the temperature range 300–1000 K the Arrhenius parameters are also very similar for the two theories in this temperature range; see Table I. At 2400 K, the conventionally calculated rate is 1.28 times larger than that calculated by canonical variational theory. For this reaction at high temperature and for other reactions with two or more dynamical bottlenecks, it would be interesting to apply the unified statistical theory of Miller.[21] However, this requires computing microcanonical cumulative reaction probabilities,[1,2] and hence it is a more difficult calculation than those reported here.

Next consider the H + AlCl reaction, which has a nearly symmetric saddle point that is only slightly closer to reactants than products. Near the saddle point of this reaction the bending frequency is a slowly varying function of reaction coordinate. Although the saddle point is near the corner-turning region of the minimum-energy path, the skew angle is large and the stretching frequency is only slowly varying with s in this region. Both frequencies increase with increasing s, and the CVT transition states are located on the product side of the saddle point. Since both frequencies are only slowly varying the maxima in the generalized free energy of activation curves in Figure 2 are located near the saddle point and have values very similar to the value at the saddle point. Thus the canonical variational theory predicts rate constants which are only 7–16% lower than conventional transition state theory in the temperature range 200–4000 K. Because the rates are so similar, so are the Arrhenius parameters.

The symmetric system Cl + CCl also has its saddle point located in the corner-turning region of the minimum-energy path. Because of the small skew angle the stretching vibration frequency dips sharply at the saddle point. However, the bending vibrational frequency is a local maximum and the moment of inertia is a local minimum at the saddle point. Thus the bending and rotational degrees of freedom as well as the classical energic Boltzmann factor favor location of the variational transition state at the saddle point. However, the stretching degree of freedom dominates the other three factors and the CVT transition state is shifted from the saddle point by 0.11, 0.11, 0.13, and $0.18a_0$ at 1, 200, 600, and 2400 K, respectively. In the generalized free energy of activation plots of Figure 3 the sharp dip in the free-energy curves at the saddle point causes the canonical variation theory rate constants to be substantially lower than the conventional one, between a

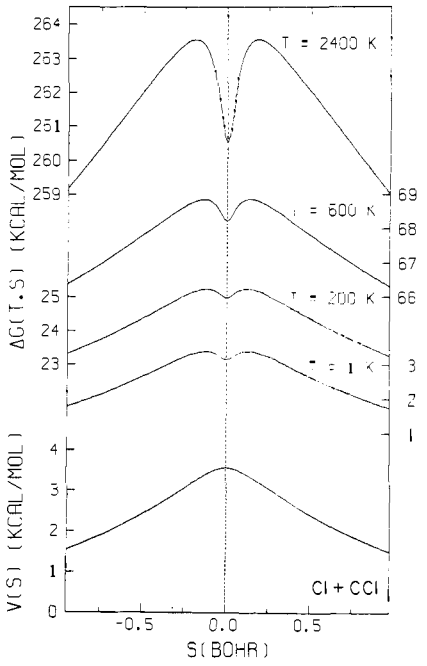

Figure 3. Same as Figure 1 except for Cl + CCl → ClC + Cl.

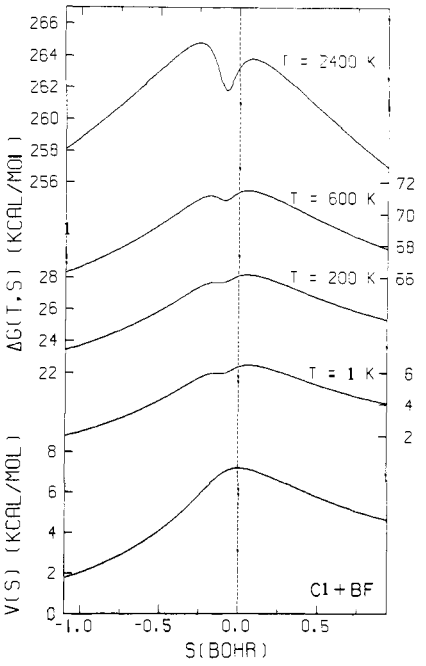

Figure 4. Same as Figure 1 except for Cl + BF → ClB + F.

factor of 1.70 and 1.93 in the temperature range 200–4000 K.

It is interesting to compare Cl + CCl to C + ClC. The latter has a much larger skew angle and the stretching vibrational frequency consequently decreases less. In particular it decreases to 520 cm^{-1} at $s = 0$ compared to 305 cm^{-1} at $s = 0$ for Cl + CCl. For both reactions the reactant and product values of the stretching frequency are 832 cm^{-1}. For C + ClC the generalized free energy of activation curves peak at $s = 0$ for 200–600 K and the effect on the calculated rate constant of varying the dividing surface location is only 4% at 2400 K and 7% at 4000 K. To make the comparison more definitive we repeated the calculation for the CClC mass combination with the ClCCl potential energy surface. Switching the surface changes the stretching frequency at $s = 0$ from 520.3 to 520.7 cm^{-1} and increases $k^{\mp}(T)/k^{CVT}(T)$ from 1.000 to only 1.001. Performing a calculation for the ClCCl mass combination with the CClC potential energy surface changes the stretching frequency at $s = 0$ from 305.0 to 304.8 cm^{-1} and decreases $k^{\mp}(T)/k^{CVT}(T)$ at 300 K from 1.71 to 1.55. This effect on $k^{\mp}(T)/k^{CVT}(T)$ is primarily due to the fact that the classical potential energy barrier increases from 3.58 to 6.16 kcal/mol; thus entropic effects compete less favorably with energetic effects for the changed calculation. The results of these two changed calculations confirm that the skew angle (which is a function only of mass combination) is indeed an important parameter in determining the effect of varying the location of the dividing surface.

Next consider the reaction Cl + BF. For this system the saddle point is located slightly to the product side of the corner-turning region of the minimum-energy path. The skew angle is small, 46°, which leads to the dips in the generalized free energy of activation curves seen in Figure 4. The stretching vibrational frequency decreases in moving from the saddle point into the corner region; the value of the stretching frequency is 1415 cm^{-1} for reactant BF, decreases to 415 cm^{-1} at $n_{ClB} = 0.55$, increases to 578 cm^{-1} at the saddle point at $n_{ClB} = 0.654$, and increases further to 846 cm^{-} for product ClB. Therefore the stretching degree of freedom favors locating the variational transition state on the product side of the saddle point. The bending frequency behaves the opposite of this near the saddle point and favors locating the dividing surface in the corner region but the effect is not large; in particular the bending frequency increases from 94 cm^{-1} at the saddle point to 98 cm^{-1} at $n_{ClB} = 0.55$. Thus the stretch dominates and the CVT transition state is shifted slightly toward products at low temperatures. For temperatures of 1500 K and higher the CVT transition state is located on the reactant side of the corner region where the stretching degree of freedom gives an even larger partition function ratio (conventional to variational). Although the earlier position of the generalized transition state yields a smaller stretching partition function even at low temperatures, it is the variationally best one only at higher temperatures where the energetic factor becomes less important and allows significantly lower potential energy at the variationally best dividing surface.

This reaction illustrates an important point about how much knowledge of the potential surface is required for variational transition state theory calculations. At low temperature, movements of the variational transition state can often be understood from the behavior of the potential surface in an expansion through cubic terms in the deviation from the saddle point; however, at higher temperature, entropic factors become relatively more important as compared to energetic factors, and there is a greater probability that the variational transition state will occur very far from the saddle point. In the present example, it occurs before the corner-turning region of the minimum-energy path, although the saddle point occurs after the corner region.

The H + BCl reaction is an example of a reaction in which neither the bending nor stretching degree of freedom dominates the classical Boltzmann factor. The saddle point is located toward products but is intermediate between the three fairly symmetric systems just considered and the systems considered below which have their saddle point far out in the asymptotic product valley. For this system the stretching degree of freedom favors locating the variational transition state further into the product region but the effect is very close in magnitude to the classical Boltzmann factor. The bending degree of freedom has a smaller effect but favors moving the variational transition state in the opposite direction, i.e., to a more symmetric geometry. Thus the classical Boltzmann factor dominates the net effect of the stretch and the bend for a variation in either direction. Because of the strong cancellation of opposing factors, the generalized free energy of activation curves (Figure 5) are very flat. Thus for this system the effects of variationally op-

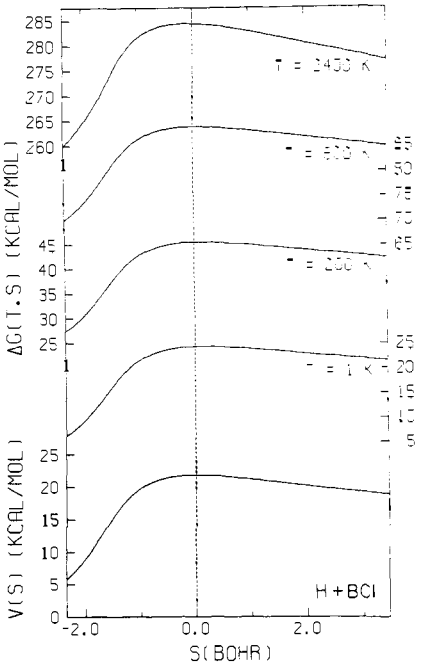

Figure 5. Same as Figure 1 except for H + BCl → HB + Cl.

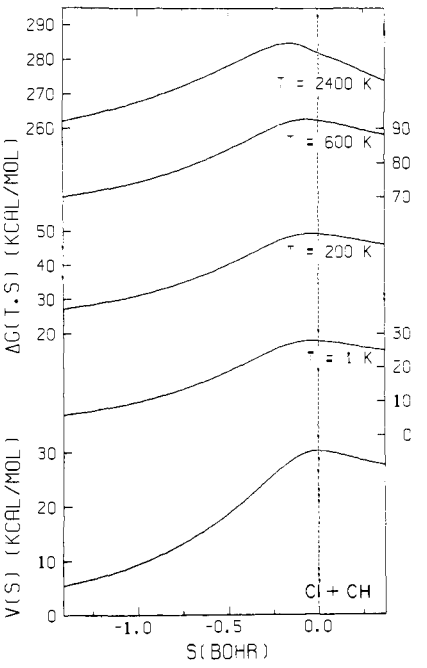

Figure 6. Same as Figure 1 except for Cl + CH → ClC + H.

timizing the dividing surface location are very small for all temperatures studied.

The Cl + CH system has its saddle point located further into the asymptotic product region than the H + BCl system, and the bending degree of freedom is more important than in the previous case. However, for this system the stretching and bending degrees of freedom both favor locating the variational transition state more toward the reactants of the endoergic reaction. For the bend this is an example of the usual trend whereby more symmetrical, i.e., tighter, generalized transition states have higher bending force constants and higher bending frequencies. For the transverse stretching mode, if the reactants and products have similar stretching frequencies, then these are both usually higher than the stretching frequency in the corner-turning region of the minimum-energy path and moving the generalized transition state away from the corner toward the endoergic product usually increases the stretching frequency which contributes to a decrease of the calculated generalized transition state theory rate. For this reaction, however, the reactant CH has a stretch frequency of 2912 cm^{-1}, and the product ClC has a stretching frequency of 832 cm^{-1}. The skew angle is large, 76°, decreasing the tendency for a dip in the stretching frequency at the corner-turning region. For this reaction the minimum of the stretching frequency occurs on the product side of the late saddle point rather than on the more symmetric side. For example, the stretching frequency is 1063 cm^{-1} at $n_{ClC} = 0.75$, 761 cm^{-1} at the saddle point at $n_{ClC} = 0.852$, and 759 and 804 cm^{-1} at $n_{CCl} = 0.90$ and 0.95, respectively. Figure 6 shows that the variational transition state is not located very far from the saddle point; it is at $n_{ClC} = 0.815$, 0.776, and 0.660 at 200, 600, and 2400 K, respectively. Nevertheless the variation of the vibrational frequencies is strong enough that the resulting rate ratios $k^{\pm}(T)/k^{CVT}(T)$ are 1.15, 1.22, and 1.82 at these three temperatures. At 2400 K, the stretching and bending degrees of freedom contribute partition function ratios of 1.95 and 1.48, respectively, to this effect. The classical potential energy and rotational degrees of freedom contribute factors of 0.65 and 0.97 to the overall product of 1.82.

The Br + OF reaction has a late saddle point and a stretching frequency that decreases from 979 cm^{-1} for reactants to 664 cm^{-1} for products, with a minimum in the corner-turning region near $n_{BrO} = 0.6$ where it is 334 cm^{-1}. The generalized free energy of activation curves, Figure 7, and the contributions of various degrees of freedom are similar in some respects to what we found for Li + HI in our previous study.[3] But there are some important differences, even qualitatively. For the Br + OF reaction the stretching and bending degrees of freedom favor moving the generalized transition state in opposite directions from the saddle point. At low temperatures the bending degree of freedom is most important in determining the dividing surface location and the CVT transition state is shifted toward reactants. The Br + OF system has a 48° skew angle causing the stretching degree of freedom to drop rapidly near the corner-turning region. On the reactant side of the corner region, the partition function ratios for both the bending and stretching degrees of freedom are greater than

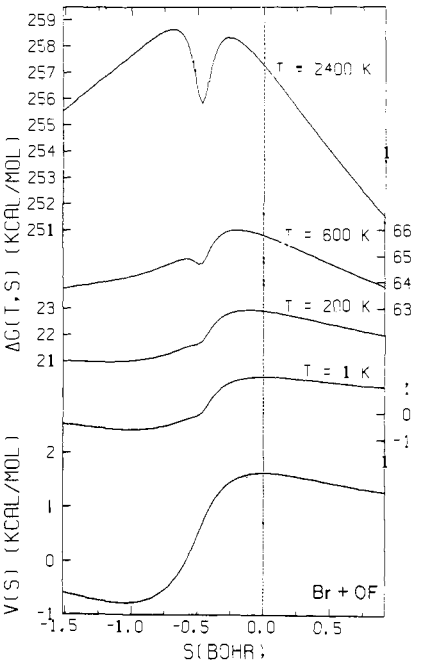

Figure 7. Same as Figure 1 except for Br + OF → BrO + F.

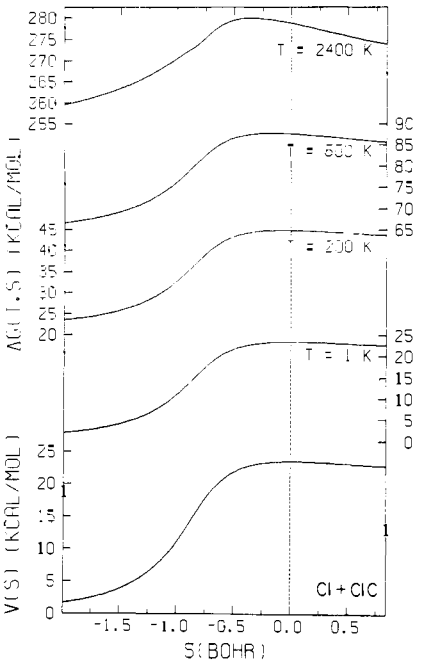

Figure 8. Same as Figure 1 except for Cl + ClC → ClCl + C.

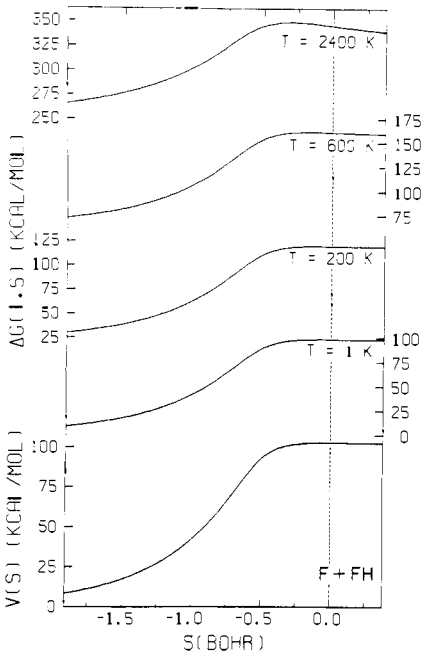

Figure 10. Same as Figure 1 except for F + FH → FF + H.

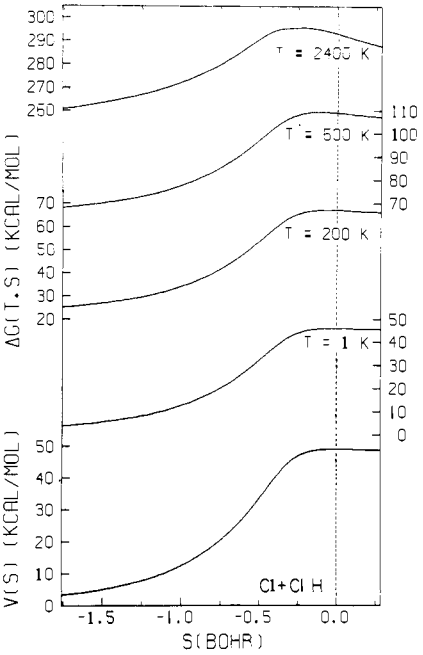

Figure 9. Same as Figure 1 except for Cl + ClH → ClCl + H.

unity. However, at low temperatures the energetic factor is very unfavorable there; only at sufficiently high temperatures (2400 K and greater) does the CVT transition state occur on the reactant side of the corner-turning region.

The final three systems considered in detail have their saddle points very far into the asymptotic product valley. These three systems, Cl + ClC, Cl + ClH, and F + FH, exhibit very similar generalized free energy of activation curves, Figures 8–10. In all three cases the bending degree of freedom dominates the stretching degree of freedom in the determination of the CVT dividing surface location at all temperatures. In all cases at low and medium temperatures the stretching degree of freedom weakly opposes the bend in determining the position of the CVT transition state, which is variationally located on the reactant side of the saddle point. However, for the Cl + ClH system at high temperatures, 2400 and 4000 K, the CVT transition state is located where the stretching degree of freedom reinforces the effect of the bending degree of freedom; see Table I. In the progression toward more asymmetric saddle points, the ratio $k^{\ddagger}(T)/k^{CVT}(T)$ increases.

Comparison to H-Atom Transfer

In the previous article[3] concerning hydrogen-atom transfers we found that, for BEBO potential energy surfaces, the dominant entropic effect upon the location of the variational dividing surface is due to the stretching degree of freedom for symmetric or near-symmetric saddle points and is due to the bending degree of freedom for relatively loose conventional transition states. For the symmetric conventional transition states the variational dividing surface is less symmetric than the saddle point, whereas for the loose conventional transition states the variational dividing surface is more symmetric than the saddle point. Here we find similar effects for transfers of heavier atoms. Again the largest differences between conventional and canonical variational transition state theory rate constants are found for the symmetric reactions and for the systems with very loose conventional transition states, and the general direction of the shift of the variational transition state locations from the conventional ones is the same as for transfers of hydrogen. For the hydrogen atom transfers the largest effects of all were found for the symmetric systems with the smallest skew angles. For the five hydrogen atom transfer reactions with symmetric conventional transition states that were considered,[3] the skew angles decreased from 60 to 18°. In the present study, because of the heavy mass of the transferred atom, the smallest skew angle for any reaction considered is only 40°. For the three symmetric reactions in this study the ratios of conventional transition state theory to canonical variational rate constants are smaller than those observed for the hydrogen atom transfer reactions with smaller skew angles. Thus the contrast with the present results makes the role of small skew angles even more clear as a principal cause of some of the effects observed for transfers of hydrogen atoms. The quasi-thermodynamic description of the important skew-angle effect is most clear for a symmetric or near-symmetric reaction involving transfer of a hydrogen atom between two heavy atoms. For such systems the frequency of the bound stretching motion tends to be very much smaller in the region where the

minimum energy path turns the corner in the r_{AB}, r_{BC} coordinate system than it is in either aymptotic region. In the corner turning region, the reaction coordinate is changing from an A–HB motion to an AH–B one, and the bound stretching motion is changing from a high-frequency A–H hydride vibration to a low-frequency A–H–B symmetric or nearly symmetric stretch and then to a high-frequency H–B hydride vibration. This corresponds to a wide, high-entropy reaction channel in the corner-turning region, and it means that a lower entropy, higher free energy bottleneck is likely to be found elsewhere. The effect can also be described in a more dynamic language. When A and B are heavy, the time scale for A–HB and AH–B motions is slower than that for hydride vibrations or, in the corner-turning region, for rapid transfer of H back and forth between the heavy atoms. This transfer back and forth has been observed in various trajectory calculations.[22] It corresponds to successive recrossings of a symmetric or nearly symmetric dividing surface and means that the fundamental recrossing assumption[23] of classical transition state theory is not well satisfied for such a dividing surface. Thus it is unlikely that such a dividing surface provides the variationally best transition state for this mass combination. Although the effect is quantitatively largest for symmetric H-atom transfers, the present paper shows that this kind of skew angle effect also largely explains the quantitative differences of conventional transition state theory from canonical variational theory for a more general class of reactions, e.g., for Cl + CCl and Cl + BF.

Concluding Remarks

The present study of 37 reactions involving the transfer of atoms other than hydrogen provides a survey of the effects of varying the location of the dividing surface on the thermal rate constants calculated by generalized transition state theory. Thermal rate constants are computed using conventional transition state theory and canonical variational theory, in both cases with quantized energy levels including anharmonicity. Comparison of the results indicates that there may be large effects of varying the location of the generalized transition state dividing surfaces for certain kinds of reactions. The largest effects in the present study are generally associated with the looser complexes. In these cases the dominant factor is the tightening of the bending motion as the dividing surface is varied to a more symmetric location. For systems with endoergicities greater than 30 kcal/mol, the average ratio[24] of the conventional transition state theory rate constant to the canonical variational theory one increases from 1.25 at 200 K to 2.53 at 4000 K.

References and Notes

(1) Garrett, B. C.; Truhlar, D. G. *J. Phys. Chem.* **1979**, *83*, 1052.
(2) Garrett, B. C.; Truhlar, D. G. *J. Phys. Chem.* **1979**, *83*, 1079. For a review see: Truhlar, D. G. *Ibid.* **1979**, *83*, 188.
(3) Garrett, B. C.; Truhlar, D. G. *J. Am. Chem. Soc.*, **1979**, *101*, 4534.
(4) Garrett, B. C.; Truhlar, D. G. *J. Phys. Chem.* **1979**, *83*, 200.
(5) Johnston, H. S.; Parr, C. A. *J. Am. Chem. Soc.* **1963**, *85*, 2444.
(6) Johnston, H. S. "Gas Phase Reaction Rate Theory", Ronald Press: New York, 1966.
(7) Mayer, S. W.; Schieler, L.; Johnston, H. S. "Eleventh Symposium (International) on Combustion", Combustion Institute: Pittsburgh, 1967; p 837.
(8) Mayer, S. W.; Schieler, L.; Johnston, H. S. *J. Chem. Phys.* **1966**, *45*, 385.
(9) Mayer, S. W.; Schieler, L. *J. Phys. Chem.* **1968**, *72*, 236.
(10) Mayer, S. W.; Schieler, L. *J. Phys. Chem.* **1968**, *72*, 2628.
(11) Rosen, B. "Spectroscopic Data Relative to Diatomic Molecules", Pergamon Press: Elmsford, N.Y., 1970.
(12) Stull, D. R., Ed. "JANAF Thermochemical Tables", Dow Chemical Co.: Midland, Mich., 1971.
(13) Herzberg, G. "Spectra of Diatomic Molecules", Van Nostrand: Princeton, N.J., 1950.
(14) Pauling, L. "The Nature of the Chemical Bond", Cornell University Press: Ithaca, N.Y., 1960.
(15) Garrett, B. C.; Turhlar, D. G. *J. Phys. Chem.*, **1979**, *83*, 1915.
(16) Hirschfelder, J. O.; Curtiss, C. F.; Bird, R. B. "Molecular Theory of Gases and Liquids", Wiley: New York, 1964.
(17) See, e.g., Previtali, C. M.; Scaiano, J. S. *J. Chem. Soc. B* **1971**, 2317.
(18) Wigner, E. P. *Z. Phys. Chem., Abt. B* **1932**, *19*, 203.
(19) Truhlar, D. G. *J. Chem. Phys.* **1972**, *56*, 3189. Erratum: **1974**, *61*, 440. Muckerman, J. T.; Newton, M. D. *J. Chem. Phys.* **1972**, *56*, 3191.
(20) Hammond, G. S. *J. Am. Chem. Soc.* **1955**, *77*, 334.
(21) Miller, W. H. *J. Chem. Phys.* **1976**, *65*, 2216.
(22) See, e.g., Pattengill, M. D.; Polanyi, J. C. *Chem. Phys.* **1974**, *3*, 1.
(23) Wigner, E. *Trans. Faraday Soc.* **1938**, *34*, 29. Miller, W. H. *J. Chem. Phys.* **1975**, *62*, 1899.

(24) This ratio is identical for the reverse exoergic reactions.

Doubly Bridged Species as Transition States or Intermediates in Transition Metal Redox Reactions

Jeremy K. Burdett

Contribution from the Department of Chemistry, The University of Chicago, Chicago, Illinois 60637. *Received March 27, 1979*

Abstract: The molecular orbital structures of symmetrically doubly bridged M_2X_{10} complexes (D_{2h}) are examined to determine for which d electron configurations this geometry is a stable intermediate or an unstable transition state. For almost all electronic configurations the structure is predicted to be stable but with a low-energy b_{3g} distortion (leading eventually to two five-coordinate units). For the remaining few configurations the structure is predicted to be unstable with decay via the b_{1u} route (leading to six- and four-coordinate units). The predictions correlate favorably with observed crystal structures. Kinetically this second result leads overall to two-ligand transfer as experimentally observed in several cases. It is pointed out that experimental detection of the one-ligand transfer route by product analysis does not exclude a doubly bridged intermediate which decays by the b_{3g} route.

Introduction

We have recently used simple molecular orbital ideas to view [1]in a fresh light the intimate mechanism of redox reactions between transition-metal ions in solution.[2-4] For inner-sphere reactions we found that whether the symmetrically bridged species **1** is an intermediate or transition state is simply determined by the electron configuration of the reacting ions M_1 and M_2. In this paper we examine the role of the doubly bridged species **2**. Experimental evidence for double bridging

0002-7863/79/1501-5217$01.00/0